



# A deformation mismatch strategy enables over 120% stretchability of encapsulated serpentine silicon strips for stretchable electronics

Yihao Shi<sup>1</sup> | Bingchang Zhang<sup>2</sup>  | Jianzhong Zhao<sup>3,4</sup> | Jiahao Qin<sup>1,5,6</sup> | Ke Bai<sup>3,4</sup> | Jia Yu<sup>1</sup> | Xiaohong Zhang<sup>1</sup> 

<sup>1</sup>Institute of Functional Nano & Soft Materials (FUNSOM), Jiangsu Key Laboratory of Advanced Negative Carbon Technologies, Soochow University, Suzhou, China

<sup>2</sup>School of Optoelectronic Science and Engineering, Key Laboratory of Advanced Optical Manufacturing Technologies of Jiangsu Province, Key Laboratory of Modern Optical Technologies of Education Ministry of China, Soochow University, Suzhou, China

<sup>3</sup>Applied Mechanics Laboratory, Department of Engineering Mechanics, Tsinghua University, Beijing, China

<sup>4</sup>Laboratory of Flexible Electronics Technology, Tsinghua University, Beijing, China

<sup>5</sup>Suzhou Industrial Park Monash Research Institute of Science and Technology, Monash University, Suzhou, China

<sup>6</sup>Department of Materials Science and Engineering, Monash University, Clayton, Victoria, Australia

## Correspondence

Bingchang Zhang, Jianzhong Zhao and Xiaohong Zhang.

Email: [zhangbingchang@suda.edu.cn](mailto:zhangbingchang@suda.edu.cn), [jianzhongzhao@tsinghua.edu.cn](mailto:jianzhongzhao@tsinghua.edu.cn) and [xiaohong\\_zhang@suda.edu.cn](mailto:xiaohong_zhang@suda.edu.cn)

## Funding information

National Natural Science Foundation of China, Grant/Award Numbers: 51821002, 51920105005, 62004134; Open Project of Key Lab of Advanced Optical Manufacturing Technologies of Jiangsu Province, Grant/Award Number: ZZ2308

## Abstract

It is significant to develop stretchable electronics based on silicon materials for practical applications. Although various stretchable silicon structures have been reported, electronic systems based on them exhibit limited stretchability due to the constraints between them and polymer substrates. Here, an innovative strategy of deformation mismatch is proposed to break the constraints between silicon structures and polymers and effectively reduce the strain concentration in silicon structures. As a result, encapsulated serpentine silicon strips (S-Si strips) achieve unprecedented stretchability, exceeding 120%. The encapsulated S-Si strip also exhibits remarkable mechanical stability and durability, enduring 100 000 cycles of 100% stretch without fracture. The effect of key parameters, including the central angle, thickness, and width of the S-Si strip, on the deformation mismatch is revealed through combing experiments and theoretical analysis, which will guide the rational implementation of the deformation mismatch strategy. Electrical testing showcases the strain-insensitive nature and good electrical stability of encapsulated S-Si strips, benefiting practical applications. This work provides a new paradigm of silicon materials with excellent stretchability and will facilitate the development of stretchable electronics.

This is an open access article under the terms of the [Creative Commons Attribution](https://creativecommons.org/licenses/by/4.0/) License, which permits use, distribution and reproduction in any medium, provided the original work is properly cited.

© 2024 The Author(s). FlexMat published by John Wiley & Sons Australia, Ltd on behalf of Nanjing University of Posts & Telecommunications.

**KEYWORDS**

deformation mismatch, encapsulated, serpentine silicon strips, stretchable electronics, stretchable silicon structures

## 1 | INTRODUCTION

Stretchable electronic systems have attracted extensive attention for their potential in various applications such as electronic skins,<sup>[1-4]</sup> implantable electronics,<sup>[5-7]</sup> and soft robots.<sup>[8-11]</sup> They can be achieved by combining stretchable electronic materials with polymer substrates.<sup>[12-15]</sup> Current research trends emphasize the exploration of stretchable electronic materials, particularly in the realm of organic materials<sup>[16-18]</sup> and hydrogels.<sup>[19,20]</sup> Despite many efforts, currently there are no widely accepted dominant materials for stretchable electronics. Silicon is one of the dominant materials in traditional electronic systems and has been widely applied in consumer electronics.<sup>[21-24]</sup> However, commonly used silicon wafers exhibit rigidity and brittleness, which make them almost unsuitable for stretchable electronic systems.<sup>[25-27]</sup>

To promote the use of silicon in stretchable electronic systems, strategies of island-bridge configuration and deformation transition have been proposed.<sup>[28]</sup> In the strategy of island-bridge configuration, non-stretchable silicon is used as the rigid island, while stretchable electrodes are employed as bridges to interconnect between the rigid islands.<sup>[29-32]</sup> Although the systems are overall stretchable through the deformation of the electrodes, the rigid islands are fragile and the interfaces are unstable under a large stretch, constraining the stretchable range of the systems.<sup>[33]</sup> In the deformation transition strategy, stretchability is endowed to silicon materials by transforming the local bending deformation into an overall stretch.<sup>[34]</sup> Stretchable silicon structures of deformation transitions can be fabricated in two different ways. On the one hand, wave-like silicon ribbons and silicon helices can be obtained through designed folding under the action of pre-strained polymers.<sup>[35-37]</sup> On the other hand, serpentine silicon structures can be directly obtained through masked etching or induced growth.<sup>[38-41]</sup> These stretchable silicon structures were integrated with polymer substrates for use in stretchable electronic systems. However, their stretchability remains below 50% (Table S1), far from meeting the demands of applications like conformal electronic skins and soft robotics, which typically require stretchability exceeding 100%.<sup>[42-45]</sup>

## 2 | RESULTS AND DISCUSSION

### 2.1 | Theoretical analysis of the deformation mismatch strategy

The limited stretchability of the above electronic systems based on stretchable silicon structures is attributed to the strain concentration and fracture of silicon structures induced by the constraints of the polymer substrates, which is confirmed with finite element analysis (FEA) (Figure 1). The elongation rate is defined as the ratio of the increase in distance between the two endpoints of the sample to the original distance. When a serpentine silicon strip (S-Si strip) is freely stretched to 60% without any constraint, the maximum strain occurs at the inner vertices of each curved beam and the value is 0.52% (Figure 1A). In contrast, the maximum strain reaches a larger value of 0.64% when an S-Si strip is bonded to a polymer substrate. It indicates that the S-Si strip integrated with a polymer substrate will suffer from strain concentration and is easier to fracture because the bonding with the polymer restricts the strip to follow the deformation mode of the polymer instead of the lowest strain energy. Nevertheless, the strain concentration will be greatly reduced if the bonding between the S-Si strip and the polymer is removed and a deformation mismatch occurs. As shown in Figure 1C, the maximum strain in the strip decreases to 0.55%, which is similar to the case of the freestanding S-Si strip. This means that the stretchability of S-Si strips integrated with polymers can be greatly improved through deformation mismatch, which has almost not been observed in previous works.

In this work, designed deformation mismatch is proposed as an effective strategy to boost the stretchability of S-Si strips integrated with polymers (i.e., encapsulated S-Si strips) by over 120%. The constraints between silicon structures and polymers can be broken through deformation mismatch, which effectively reduces the strain concentration in silicon structures and enables them to withstand large stretching. The encapsulated S-Si strip also exhibits remarkable mechanical stability and durability, enduring 100 000 cycles of 100% stretch without fracture. This strategy provides a new route to solve the problem of excessive constraints and strain concentration

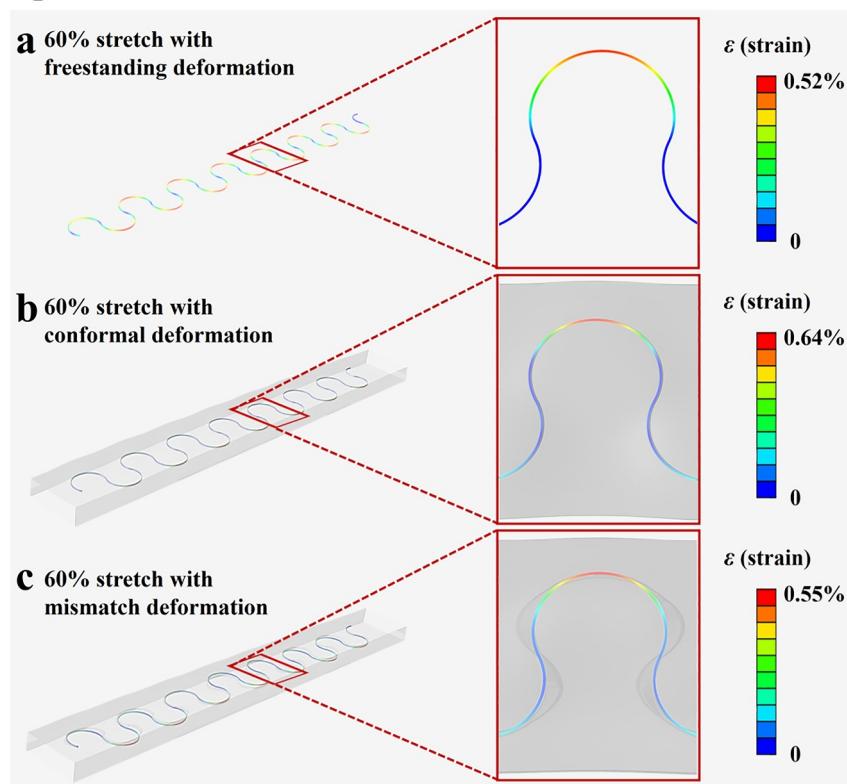


**FIGURE 1** Finite element analysis of the strain distribution in stretched S-Si strips. (A) The strain distribution of an S-Si strip stretched to 60% freely. (B) The strain distribution of an encapsulated S-Si strip with interface bonding stretched to 60%. (C) The strain distribution of an encapsulated S-Si strip without interface bonding stretched to 60%.

in hybrid stretchable systems and will promote the wide applications of S-Si strips in stretchable electronics.

## 2.2 | Experimental research on the stretchability and robustness of encapsulated S-Si strips

S-Si strips are prepared through dry etching masked by photolithography (Figure 2A). First, a resist layer is patterned onto a silicon-on-insulator (SOI) wafer. The exposed top layer of silicon is removed in a deep reactive ion etching (RIE) process. After eliminating residual photoresist with acetone, the buried oxide layer is etched with hydrofluoric acid to liberate the S-Si strip from the underlying silicon substrate. Then, the S-Si strips are transferred onto a cured Ecoflex substrate, followed by casting uncured Ecoflex to complete the encapsulation process. Figure 2B shows the SEM images of typical S-Si strips fabricated from SOI wafers with a top silicon layer thickness of 30  $\mu\text{m}$ .

Deformation mismatch can occur through stretching the encapsulated S-Si strip to a critical elongation rate of 50%–60% (Figure 2C). The corresponding microscopic images show that the S-Si strip undergoes conformal deformation with the polymer under a small elongation

rate of 40%, while the process of deformation mismatch between the S-Si strip and the polymer can be observed as the stretch exceeds 60% (Figure 2D–F). In Figure 2F, the black line is the S-Si strip and the bright white line represents a side of the polymer trench. The S-Si strip is obviously separated from the side of the polymer trench under the elongation rate of 70%, reflecting the complete deformation mismatch.

With deformation mismatch, the encapsulated S-Si strip can be stretched to 100% without fracture (Figure 3A). The stretch limit reaches over 120%, where fracture of the S-Si strip occurs (Figure S1). Moreover, it is noted that after the encapsulated S-Si strip is stretched over the critical elongation at the first stretch, the deformation mode at the subsequent stretch is different from that at the first stretch. As shown in Figure 3B, the encapsulated S-Si strip recovers to its original status without apparent structural misalignment when the elongation rate is reduced to 0% after the first stretch. In the subsequent stretches, deformation mismatch will occur, no matter under a little or large stretch (Figure 3B–D). This is because the interface between the S-Si strip and the polymer is irreversible, and the reduced constraint allows the structure to deform in the form of the lowest strain energy. In addition, stretching of 100 000 cycles at a 100% elongation rate was performed on an encapsulated S-Si strip

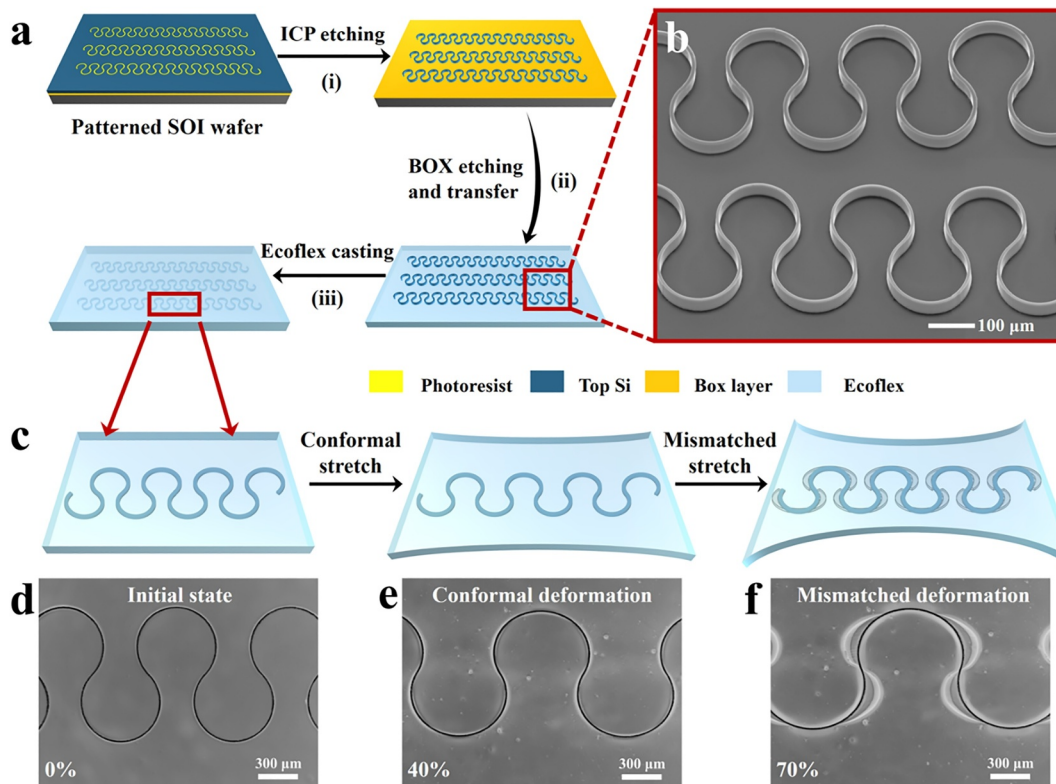


**FIGURE 2** Fabrication and characterization of S-Si strips. (A) Schematic illustration of the processes for fabricating encapsulated S-Si strips. (B) SEM images of S-Si strips on an Ecoflex substrate. (C) The illustration of the first-time tensile process of encapsulated strips. (D–F) The microscopic images of an encapsulated S-Si strip at elongation rates of (D) 0%, (E) 40%, and (F) 70% in its first-time tensile process.

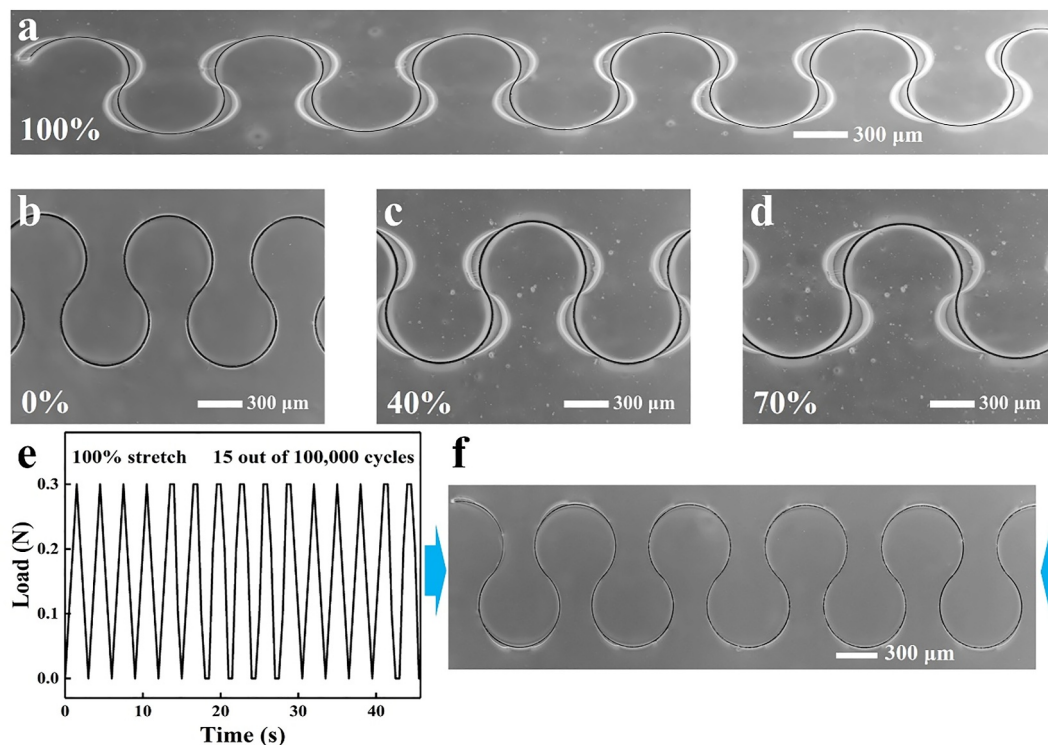


**FIGURE 3** The stretching performance of the encapsulated S-Si strip. (A) The microscopic image of an encapsulated S-Si strip at an elongation rate of 100%. (B–D) The microscopic image of an encapsulated S-Si strip stretched to (B) 0%, (C) 40%, and (D) 70% after deformation mismatch. (E) 15-cycle loading curve of an encapsulated S-Si strip from 100 000 cycles of 100% stretch. (F) The microscopic image of the encapsulated S-Si strip recovered to its initial state after 100 000 cycles of 100% stretch.

(Figure 3E and Figure S2). The structure remained stable without fracture and recovered to its original state after all the cycles (Figure 3F), demonstrating the outstanding durability of the encapsulated S-Si strip. Furthermore, the deformation of the Si strip embedded zone is found consistent with that of the corresponding region in a homogenous Ecoflex elastomeric polymer, indicating that the embedding of S-Si strips has no discernible effect on the deformation behavior of the polymer (Figure S3).

### 2.3 | Effect of the central angle on the stretchability of encapsulated S-Si strips

Although encapsulated S-Si strips with stretchability over 100% can be achieved through the deformation mismatch

strategy, it is noted that deformation mismatch is dependent on the structure parameters. The central angle of the curved beam ( $\theta$ ) in the S-Si strip is an important parameter that impacts the deformation form and strain concentration of encapsulated S-Si strips. S-Si strips with central angles of  $1.3\pi$ ,  $1.4\pi$ ,  $1.5\pi$ , and  $1.6\pi$  were prepared and subjected to encapsulated stretching tests until fracture (Figure 4A). Only S-Si strips with a central angle of  $1.5\pi$  experienced a deformation mismatch after completing 60% of conformal deformation, ultimately reaching an elongation rate of 123%. In contrast, S-Si strips with central angles of  $1.3\pi$ ,  $1.4\pi$ , and  $1.6\pi$  fractured at elongation rates of 42%, 47%, and 33%, respectively, and no deformation mismatch occurred. In addition, the fractures first occur at the vertexes of each curved beam for all the samples

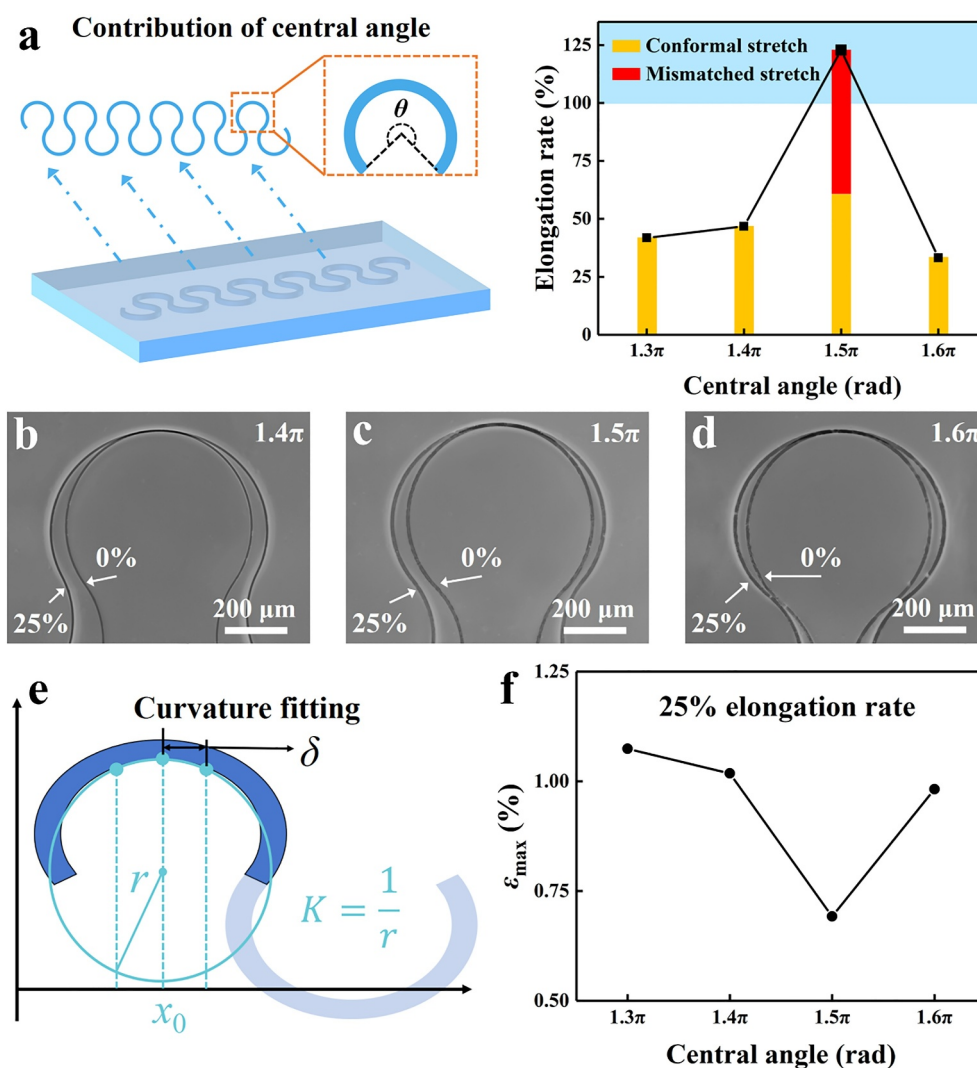


**FIGURE 4** The effect of the central angle on the stretch limit of encapsulated S-Si strips. (A) The relationship between the stretch limit and the central angle of encapsulated S-Si strips. (B–D) The overlapped photographs of encapsulated S-Si strips with central angles of (B)  $1.4\pi$ , (C)  $1.5\pi$ , and (D)  $1.6\pi$  at 0% and 25% elongation rate. (E) The illustration of the curvature fitting. (F) The relationship between the maximum strain at the inner vertex and the central angle of encapsulated S-Si strips at a 25% elongation rate.

(Figure S4), indicating strong strain concentration in these positions.

To explore the reasons for different stretchability, microscopic images of S-Si strips with different central angles at 0% and 25% elongation rates were overlapped (Figure 4B–D and Figure S5). It is observed that both the overall deformation of the S-Si strips and the local bending deformation around the vertexes are very different. For encapsulated S-Si strips at a 25% elongation rate, the inner curvatures  $\kappa_2$  of the vertexes are fitted by drawing a circle through the vertex and 50  $\mu\text{m}$  points on the left and right sides of the vertex (Figure 4E). The maximum tensile strain at the inner vertex of the curved beam can be expressed as follows:<sup>[46]</sup>

$$\varepsilon = \frac{1}{2}(\kappa_2 - \kappa_1)w, \quad (1)$$

where  $\kappa_1$  is the initial curvature of the undeformed S-Si strip and  $w$  is the track width. By substituting the fitted  $\kappa_2$  into Equation (1), the maximum tensile strains for S-Si strips with different central angles are calculated and depicted in Figure 4F. The maximum tensile strains for S-Si strips with central angles of  $1.3\pi$ ,  $1.4\pi$ , and  $1.6\pi$  at a 25% elongation rate are 1.07%, 1.01%, and 0.98%, respectively. It means that the maximum tensile strains in these samples will quickly approach the 1.25% fracture strain of silicon when continuously stretching from the 25% elongation rate. Therefore, the stretch limit of these samples has relatively small values of 30%–50%. In contrast, the maximum tensile strain for the S-Si strip with a central angle of  $1.5\pi$  is 0.69%, obviously lower than those for the other samples. This strip can be conformally stretched to 60% without fracture. When the encapsulated S-Si strip was further stretched from the 60% elongation rate, a deformation mismatch between the strip and the polymer occurred. The deformation mismatch further decreased the strain concentration in the S-Si strip and resulted in a 123% stretch limit.

The experimental performances of encapsulated S-Si strips with different central angles can be understood as follows: deformation mismatch occurs when the pulling force at the interface of the S-Si strip and the polymer is large enough to separate them (Video S1). The pulling force at the interface is positively related to the elongation rate of the sample because the difference in deformation modes between the S-Si strip and the polymer increases with the increase in the elongation rate. As a result, the occurrence of a deformation mismatch requires a critical elongation rate, such as 60% for the sample with a central angle of  $1.5\pi$ . Nevertheless, the S-Si strips with other central angles fracture at a small elongation rate of 30%–50%, smaller than the critical

elongation rate. Therefore, deformation mismatch is difficult to occur in these samples.

## 2.4 | Effect of the width and thickness on the stretchability of encapsulated S-Si strips

The occurrence of deformation mismatch in encapsulated S-Si strips is also related to the in-plane bending stiffness of Si beams. A larger difference in the stiffness between the Si beam and the polymer will result in an easier deformation mismatch. The in-plane bending stiffness ( $k$ ) of a Si beam can be expressed as follows:<sup>[47]</sup>

$$k = EI = \frac{Ew^3t}{12}, \quad (2)$$

where  $E$  is the Young's modulus,  $I$  is the in-plane moment of inertia, and  $t$  is the structural thickness. The track width ( $w$ ) and structural thickness ( $t$ ) are crucial in determining the bending stiffness of the Si beams,<sup>[48]</sup> which are further investigated in detail, respectively. In the following studies, the central angle of the S-Si strip is set at the optimal value of  $1.5\pi$ .

On the one hand, S-Si strips with  $t$  of 0.1, 2, 10, and 30  $\mu\text{m}$  were prepared and subjected to encapsulated stretching tests (Figure 5A). When the thickness of the S-Si strip is small (e.g.,  $\leq 2\mu\text{m}$ ), the in-plane bending stiffness is small, and it is easy for the S-Si strip to undergo strain concentration induced by the polymer. Therefore, the S-Si strip fractures at a small elongation rate and cannot reach the critical elongation rate for deformation mismatch. In contrast, when the thickness of the S-Si strip is greater than 10  $\mu\text{m}$ , the bending stiffness is sufficient to support S-Si strips to resist the deformation induction of the polymer. The sample will not fracture before the critical elongation rate and will undergo a deformation mismatch after that. The stretch limit of these samples reaches over 100% and increases with the increase in thickness.

On the other hand, S-Si strips with  $t$  of 10  $\mu\text{m}$  and  $w$  of 2.5, 5, 7.5, and 10  $\mu\text{m}$  were prepared and subjected to encapsulated stretching tests (Figure 5B). No deformation mismatch is observed for encapsulated S-Si strips with  $w$  of 2.5, 5 and 7.5  $\mu\text{m}$  due to the insufficient bending stiffness. Moreover, the stretch limit gradually decreases with the increase of  $w$  from 2.5 to 7.5  $\mu\text{m}$  because the maximum tensile strain at the inner vertex of the curved beam increases with the increase of  $w$  (Equation (1)). On the other hand, for the encapsulated S-Si strip with  $w$  of 10  $\mu\text{m}$ , the bending stiffness is large enough to make it reach the critical elongation rate and undergo

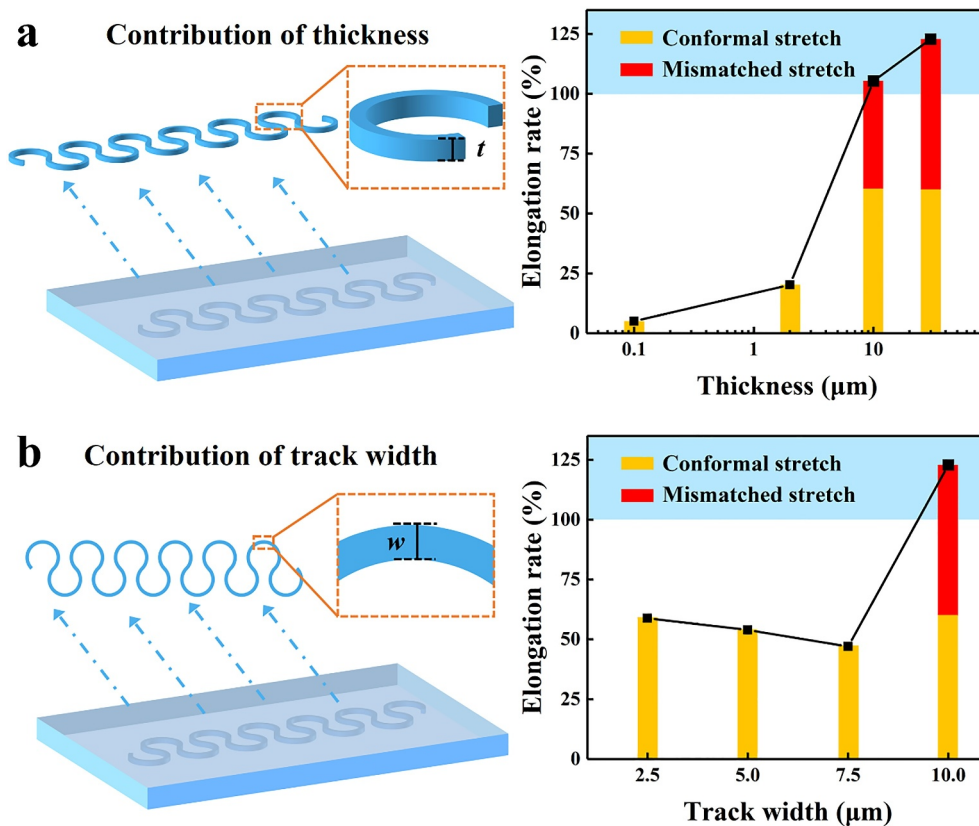


**FIGURE 5** The effect of the thickness and track width on the stretch limit of encapsulated S-Si strips. (A) The relationship between the stretch limit and the thickness of encapsulated S-Si strips. (B) The relationship between the stretch limit and the track width of encapsulated S-Si strips.

deformation mismatch. The above results indicate that the deformation mismatch strategy can be effectively achieved through modulating the central angles to change the deformation mode of the S-Si strip, as well as designing its thickness and width to increase the bending stiffness of the Si beam.

## 2.5 | Electrical stability of encapsulated S-Si strips

Finally, the effect of mismatched deformation on the electrical properties of encapsulated S-Si strips was evaluated. The electrical signal testing device was fabricated by integrating an S-Si strip with two serpentine copper/polyimide electrodes at both ends and leading out with copper wires, before encapsulation with Ecoflex (Figure 6A,B). When stretching the device at elongation rates of 0%, 20%, 40%, 60%, 80%, and 100%, the  $I$ - $V$  curves under a bias voltage of  $-5$ - $5$  V were tested, respectively (Figure 6C). The curves at different elongation rates are almost consistent, and the changing ratio of the current at any specific bias voltage is less than 2%, representing a strain-insensitive electrical property of the encapsulated

S-Si strip. Although the electrical resistances of the S-Si strip at different elongation rates show a small difference, they are negatively correlated to the elongation rates. Figure 6D shows the electrical resistance of an S-Si strip at the first three stretching cycles. At a specific elongation rate, the electrical resistances in the three stretching cycles show a little difference of less than 0.5%, which may come from instrumental error or environmental disturbance. The results indicate the good electrical stability of the encapsulated S-Si strip. The strain-insensitive electrical property and good electrical stability will benefit the applications of encapsulated S-Si strips in stretchable electronics.

## 3 | CONCLUSION

In conclusion, this work reports a deformation mismatch strategy to enable over 120% stretchability of encapsulated S-Si strips. After stretching to a critical elongation rate, a deformation mismatch between the S-Si strip and the polymer occurs, which greatly reduces the strain concentration in the strip and benefits its large stretchability. The encapsulated S-Si strip exhibits excellent

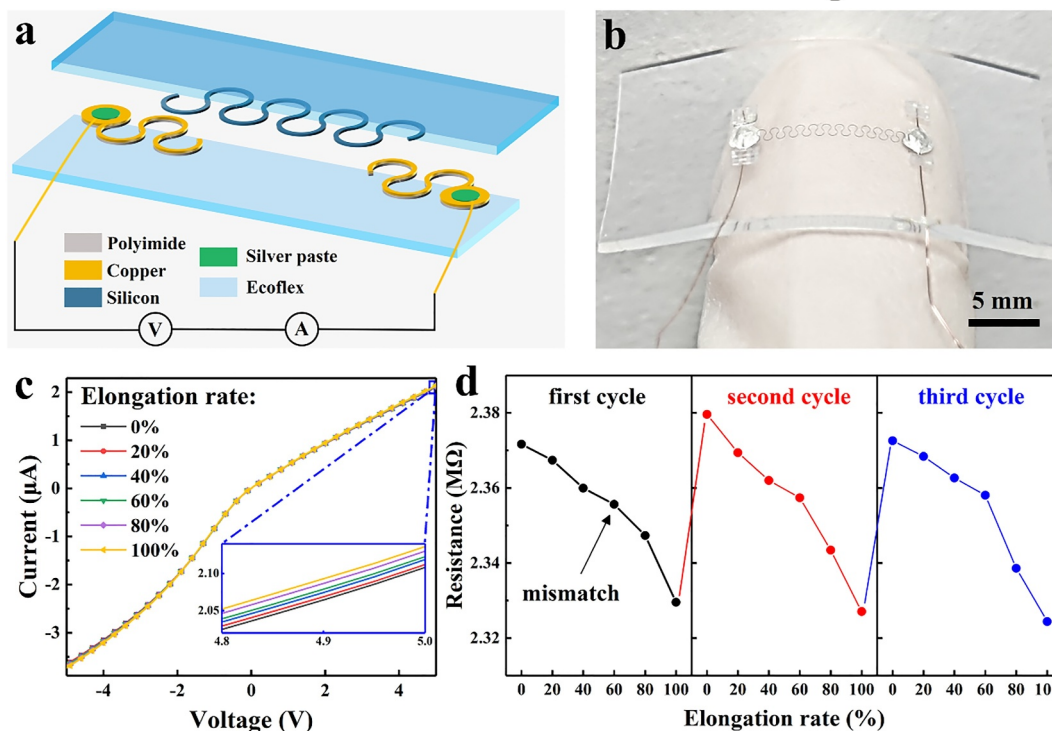


**FIGURE 6** The characterization of the electrical properties of encapsulated S-Si strips. (A) The illustration of the electrical signal testing device. (B) A photograph of an electrical signal testing device based on the S-Si strip. (C) The  $I$ - $V$  curves of the device stretched to 0, 20, 40, 60, 80, and 100%. (D) The resistance-elongation rate curves of the device stretched to 0, 20, 40, 60, 80, and 100% for three cycles.

stability and durability in 100 000 cycles of 100% stretch. The key parameters that impact the occurrence of deformation mismatches are investigated by combining experiments and theoretical analysis. The results indicate that modulating the central angles of the S-Si strip to change its deformation form and designing its thickness and width to increase the bending stiffness are both effective for achieving the deformation mismatch strategy. Finally, the strain-insensitive electrical property and good electrical stability of the encapsulated S-Si strip are demonstrated. The deformation mismatch strategy provides a new route to solve the problem of excessive constraints and strain concentration in hybrid stretchable systems and will promote the wide applications of stretchable silicon structures in stretchable electronics.

## 4 | EXPERIMENTAL SECTION

### 4.1 | Fabrication of encapsulated S-Si strips

Serpentine Si strips were fabricated from SOI wafers (top Si layer of 0.1, 2, 10, and 30  $\mu\text{m}$ , p-type doping, resistivity

of 1–10  $\Omega\text{-cm}$ , and buried oxide of 3  $\mu\text{m}$  thick). The wafers were patterned by photolithography using AZ 4620 photoresist and etched with deep RIE. The etching process was set with a  $\text{SF}_6$  flow rate of 450 sccm and a  $\text{C}_4\text{F}_8$  flow rate of 190 sccm in a Bosch process. After the photoresist was washed away with N-methyl-2-pyrrolidone (NMP), the buried oxide layer was then etched in HF (40%) to release S-Si strips. The encapsulated S-Si strips were cast with Ecoflex-0031 silicone rubber (Smooth-On, USA). SEM images of S-Si strips were acquired with a Hitachi SU5000 scanning electron microscope.

### 4.2 | Durability test of encapsulated S-Si strips

The cyclic tensile testing relied on a NanoUp FlexTest-TM-L system, combined with the FlexTest-S-P2 module. The stretching length was set to the distance between the clamping points at both ends of the encapsulated S-Si strip (100% elongation rate). The running time of a single cycle and the pause time between cycles were set to 2 and 1 s, respectively.

### 4.3 | Fabrication and test of electrical testing devices

The device was fabricated by depositing 50 nm gold onto both ends of the S-Si strips through electron-beam evaporation with a metal mask. The gold parts were in conformal contact with serpentine copper—polyimide (PI) strips and extended using silver paste and copper wires. The electrical test was performed with a digital source meter (Keithley 2636B). The device was stretched using a mechanical displacement platform (Figure S6).

### 4.4 | Finite element analysis

FEA was conducted with the commercial software ABAQUS, version 2021. The S-Si strips were modeled by four-node shell elements (S4R). The silicon was modeled by linear elastic solids, with material properties of 130 GPa (Young's modulus) and 0.27 (Poisson's ratio). The Ecoflex was built as an isotropic hyper-elastic model based on the Mooney–Rivlin law, where the effective elastic modulus and Poisson's ratio were given as 0.05 MPa and 0.49, respectively. The initial disturbance was set sufficiently small to ensure the accuracy of the simulation results.

#### AUTHOR CONTRIBUTIONS

**Yihao Shi:** Data curation; formal analysis; investigation; methodology; validation; visualization; writing – original draft. **Bingchang Zhang:** Conceptualization; formal analysis; funding acquisition; project administration; supervision; validation; writing – review & editing. **Jianzhong Zhao:** Formal analysis; methodology. **Jiahao Qin:** Methodology. **Ke Bai:** Investigation. **Jia Yu:** Project administration. **Xiaohong Zhang:** Funding acquisition; resources; supervision; writing – review & editing.

#### ACKNOWLEDGMENTS

This work was financially supported by the Foundation for Innovation Research Groups of the National Natural Science Foundation of China (Grant No. 51821002), the Major International (Regional) Joint Research Project of the National Natural Science Foundation of China (Grant No. 51920105005), the National Natural Science Foundation of China (Grant No. 62004134), the Open Project of Key Lab of Advanced Optical Manufacturing Technologies of Jiangsu Province (ZZ2308), the Suzhou Key Laboratory of Functional Nano & Soft Materials, the Collaborative Innovation Center of Suzhou Nano Science and Technology, the Priority Academic Program Development of Jiangsu Higher Education Institutions (PAPD), the 111 Project, and the Joint International

Research Laboratory of Carbon-Based Functional Materials and Devices.

#### CONFLICT OF INTEREST STATEMENT

The authors declare no conflict of interests.

#### DATA AVAILABILITY STATEMENT

The data that support the findings of this study are available from the corresponding author upon reasonable request.

#### ORCID

Bingchang Zhang  <https://orcid.org/0000-0003-0520-1058>

Xiaohong Zhang  <https://orcid.org/0000-0002-6732-2499>

#### REFERENCES

1. W. Wang, Y. Jiang, D. Zhong, Z. Zhang, S. Choudhury, J.-C. Lai, H. Gong, S. Niu, X. Yan, Y. Zheng, C.-C. Shih, R. Ning, Q. Lin, D. Li, Y.-H. Kim, J. Kim, Y.-X. Wang, C. Zhao, C. Xu, X. Ji, Y. Nishio, H. Lyu, J. B. H. Tok, Z. Bao, *Science* **2023**, *380*, 735.
2. C. Wang, B. Qi, M. Lin, Z. Zhang, M. Makihata, B. Liu, S. Zhou, Y.-h. Huang, H. Hu, Y. Gu, Y. Chen, Y. Lei, T. Lee, S. Chien, K.-I. Jang, E. B. Kistler, S. Xu, *Nat. Biomed. Eng.* **2021**, *5*, 749.
3. E. Shirzaei Sani, C. Xu, C. Wang, Y. Song, J. Min, J. Tu, S. A. Solomon, J. Li, J. L. Banks, D. G. Armstrong, W. Gao, *Sci. Adv.* **2023**, *9*, eadf7388.
4. S. Huang, B. Zhang, Z. Shao, L. He, Q. Zhang, J. Jie, X. Zhang, *Nano Lett.* **2020**, *20*, 2478.
5. Y. Jiang, S. Ji, J. Sun, J. Huang, Y. Li, G. Zou, T. Salim, C. Wang, W. Li, H. Jin, J. Xu, S. Wang, T. Lei, X. Yan, W. Y. X. Peh, S.-C. Yen, Z. Liu, M. Yu, H. Zhao, Z. Lu, G. Li, H. Gao, Z. Liu, Z. Bao, X. Chen, *Nature* **2023**, *614*, 456.
6. L. Tian, B. Zimmerman, A. Akhtar, K. J. Yu, M. Moore, J. Wu, R. J. Larsen, J. W. Lee, J. Li, Y. Liu, B. Metzger, S. Qu, X. Guo, K. E. Mathewson, J. A. Fan, J. Cornman, M. Fatina, Z. Xie, Y. Ma, J. Zhang, Y. Zhang, F. Dolcos, M. Fabiani, G. Gratton, T. Bretl, L. J. Hargrove, P. V. Braun, Y. Huang, J. A. Rogers, *Nat. Biomed. Eng.* **2019**, *3*, 194.
7. J. C. Yang, J. Mun, S. Y. Kwon, S. Park, Z. Bao, S. Park, *Adv. Mater.* **2019**, *31*, 1904765.
8. Q. Shen, M. Jiang, R. Wang, K. Song, M. H. Vong, W. Jung, F. Krisnadi, R. Kan, F. Zheng, B. Fu, P. Tao, C. Song, G. Weng, B. Peng, J. Wang, W. Shang, M. D. Dickey, T. Deng, *Science* **2023**, *379*, 488.
9. Y. Bai, H. Wang, Y. Xue, Y. Pan, J.-T. Kim, X. Ni, T.-L. Liu, Y. Yang, M. Han, Y. Huang, J. A. Rogers, X. Ni, *Nature* **2022**, *609*, 701.
10. Y. Lee, J. W. Chung, G. H. Lee, H. Kang, J.-Y. Kim, C. Bae, H. Yoo, S. Jeong, H. Cho, S.-G. Kang, J. Y. Jung, D.-W. Lee, S. Gam, S. G. Hahm, Y. Kuzumoto, S. J. Kim, Z. Bao, Y. Hong, Y. Yun, S. Kim, *Sci. Adv.* **2021**, *7*, eabg9180.
11. Y. D. Horev, A. Maity, Y. Zheng, Y. Milyutin, M. Khatib, M. Yuan, R. Y. Suckeveriene, N. Tang, W. Wu, H. Haick, *Adv. Mater.* **2021**, *33*, 2102488.

12. Q. Hua, G. Shen, *Chem. Soc. Rev* **2024**, *53*, 1316.
13. D. Qi, K. Zhang, G. Tian, B. Jiang, Y. Huang, *Adv. Mater.* **2021**, *33*, 2003155.
14. H. Song, G. Luo, Z. Ji, R. Bo, Z. Xue, D. Yan, F. Zhang, K. Bai, J. Liu, X. Cheng, W. Pang, Z. Shen, Y. Zhang, *Sci. Adv.* **2022**, *8*, eabm3785.
15. S. Wang, J. Xu, W. Wang, G. N. Wang, R. Rastak, F. Molina-Lopez, J. W. Chung, S. Niu, V. R. Feig, J. Lopez, T. Lei, S. K. Kwon, Y. Kim, A. M. Foudeh, A. Ehrlich, A. Gasperini, Y. Yun, B. Murmann, J. B. Tok, Z. Bao, *Nature* **2018**, *555*, 83.
16. H. Lee, Z. Jiang, T. Yokota, K. Fukuda, S. Park, T. Someya, *Mater. Sci. Eng. R Rep.* **2021**, *146*, 100631.
17. J. S. Park, G.-U. Kim, S. Lee, J.-W. Lee, S. Li, J.-Y. Lee, B. J. Kim, *Adv. Mater.* **2022**, *34*, 2201623.
18. J. Chen, W. Huang, D. Zheng, Z. Xie, X. Zhuang, D. Zhao, Y. Chen, N. Su, H. Chen, R. M. Pankow, Z. Gao, J. Yu, X. Guo, Y. Cheng, J. Strzalka, X. Yu, T. J. Marks, A. Facchetti, *Nat. Mater.* **2022**, *21*, 564.
19. M. A. Gonzalez, J. R. Simon, A. Ghoorchian, Z. Scholl, S. Lin, M. Rubinstein, P. Marszalek, A. Chilkoti, G. P. López, X. Zhao, *Adv. Mater.* **2017**, *29*, 1604743.
20. C. Xu, Y. Sun, J. Zhang, W. Xu, H. Tian, *Adv. Energy Mater.* **2022**, *12*, 2201542.
21. D. Akinwande, C. Huyghebaert, C.-H. Wang, M. I. Serna, S. Goossens, L.-J. Li, H. S. P. Wong, F. H. L. Koppens, *Nature* **2019**, *573*, 507.
22. F. Priolo, T. Gregorkiewicz, M. Galli, T. F. Krauss, *Nat. Nanotechnol.* **2014**, *9*, 19.
23. B.-C. Zhang, Y.-H. Shi, J. Mao, S.-Y. Huang, Z.-B. Shao, C.-J. Zheng, J.-S. Jie, X.-H. Zhang, *Adv. Mater.* **2021**, *33*, 2008171.
24. T. Wei, Y. Shi, B. Zhang, Y. Ding, J. Qin, X. Hu, J. Yu, R. Liu, X. Zhang, *J. Mater. Chem. C* **2024**, *12*, 5826.
25. D.-M. Sun, M. Y. Timmermans, A. Kaskela, A. G. Nasibulin, S. Kishimoto, T. Mizutani, E. I. Kauppinen, Y. Ohno, *Nat. Commun.* **2013**, *4*, 2302.
26. S. Suthram, J. C. Ziegert, T. Nishida, S. E. Thompson, *IEEE Electron Device Lett.* **2007**, *28*, 58.
27. H. Zhang, J. Tersoff, S. Xu, H. Chen, Q. Zhang, K. Zhang, Y. Yang, C.-S. Lee, K.-N. Tu, J. Li, Y. Lu, *Sci. Adv.* **2016**, *2*, e1501382.
28. D.-H. Kim, J.-H. Ahn, W. M. Choi, H.-S. Kim, T.-H. Kim, J. Song, Y. Y. Huang, Z. Liu, C. Lu, J. A. Rogers, *Science* **2008**, *320*, 507.
29. R. Libanori, R. M. Erb, A. Reiser, H. Le Ferrand, M. J. Süess, R. Spolenak, A. R. Studart, *Nat. Commun.* **2012**, *3*, 1265.
30. N. Matsuhisa, M. Kaltenbrunner, T. Yokota, H. Jinno, K. Kuribara, T. Sekitani, T. Someya, *Nat. Commun.* **2015**, *6*, 7461.
31. J. C. Yang, S. Lee, B. S. Ma, J. Kim, M. Song, S. Y. Kim, D. W. Kim, T.-S. Kim, S. Park, *Sci. Adv.* **2022**, *8*, eabn3863.
32. D.-H. Kim, N. Lu, R. Ma, Y.-S. Kim, R.-H. Kim, S. Wang, J. Wu, S. M. Won, H. Tao, A. Islam, K. J. Yu, T.-i. Kim, R. Chowdhury, M. Ying, L. Xu, M. Li, H.-J. Chung, H. Keum, M. McCormick, P. Liu, Y.-W. Zhang, F. G. Omenetto, Y. Huang, T. Coleman, J. A. Rogers, *Science* **2011**, *333*, 838.
33. W. Wang, S. Wang, R. Rastak, Y. Ochiai, S. Niu, Y. Jiang, P. K. Arunachala, Y. Zheng, J. Xu, N. Matsuhisa, X. Yan, S.-K. Kwon, M. Miyakawa, Z. Zhang, R. Ning, A. M. Foudeh, Y. Yun, C. Linder, J. B. H. Tok, Z. Bao, *Nat. Electron.* **2021**, *4*, 143.
34. Y. Zhang, S. Xu, H. Fu, J. Lee, J. Su, K. C. Hwang, J. A. Rogers, Y. Huang, *RSC Soft Matter* **2013**, *9*, 8062.
35. D.-Y. Khang, H. Jiang, Y. Huang, J. A. Rogers, *Science* **2006**, *311*, 208.
36. Y. Sun, W. M. Choi, H. Jiang, Y. Y. Huang, J. A. Rogers, *Nat. Nanotechnol.* **2006**, *1*, 201.
37. S. Xu, Z. Yan, K.-I. Jang, W. Huang, H. Fu, J. Kim, Z. Wei, M. Flavin, J. McCracken, R. Wang, A. Badea, Y. Liu, D. Xiao, G. Zhou, J. Lee, H. U. Chung, H. Cheng, W. Ren, A. Banks, X. Li, U. Paik, R. G. Nuzzo, Y. Huang, Y. Zhang, J. A. Rogers, *Science* **2015**, *347*, 154.
38. J. Kim, M. Lee, H. J. Shim, R. Ghaffari, H. R. Cho, D. Son, Y. H. Jung, M. Soh, C. Choi, S. Jung, K. Chu, D. Jeon, S. T. Lee, J. H. Kim, S. H. Choi, T. Hyeon, D. H. Kim, *Nat. Commun.* **2014**, *5*, 5747.
39. H. Ma, R. Yuan, J. Wang, Y. Shi, J. Xu, K. Chen, L. Yu, *Nano Lett.* **2020**, *20*, 5072.
40. Z. Xue, M. Sun, T. Dong, Z. Tang, Y. Zhao, J. Wang, X. Wei, L. Yu, Q. Chen, J. Xu, Y. Shi, K. Chen, P. Roca i Cabarrocas, *Nano Lett.* **2017**, *17*, 7638.
41. R. Yuan, W. Qian, Z. Liu, J. Wang, J. Xu, K. Chen, L. Yu, *Small* **2022**, *18*, 2104690.
42. G. Chen, N. Matsuhisa, Z. Liu, D. Qi, P. Cai, Y. Jiang, C. Wan, Y. Cui, W. R. Leow, Z. Liu, S. Gong, K. Q. Zhang, Y. Cheng, X. Chen, *Adv. Mater.* **2018**, *30*, e1800129.
43. H. Liu, S. Zhang, Z. Li, T. J. Lu, H. Lin, Y. Zhu, S. Ahadian, S. Emaminejad, M. R. Dokmeci, F. Xu, A. Khademhosseini, *Matter* **2021**, *4*, 2886.
44. Q. Guo, M. Zhang, Z. Xue, G. Wang, D. Chen, R. Cao, G. Huang, Y. Mei, Z. Di, X. Wang, *Small* **2015**, *11*, 4140.
45. G. Li, Z. Ma, C. You, G. Huang, E. Song, R. Pan, H. Zhu, J. Xin, B. Xu, T. Lee, Z. An, Z. Di, Y. Mei, *Sci. Adv.* **2020**, *6*, eaaz6511.
46. E. L. White, J. C. Case, R. K. Kramer, *Sens. Actuators, A* **2017**, *253*, 188.
47. Y. Zhang, H. Fu, S. Xu, J. A. Fan, K.-C. Hwang, J. Jiang, J. A. Rogers, Y. Huang, *J. Mech. Phys. Solids* **2014**, *72*, 115.
48. Y. Shi, J. Zhao, B. Zhang, J. Qin, X. Hu, Y. Cheng, J. Yu, J. Jie, X. Zhang, *Adv. Mater.* **2024**, 2313603.

## SUPPORTING INFORMATION

Additional supporting information can be found online in the Supporting Information section at the end of this article.

**How to cite this article:** Y. Shi, B. Zhang, J. Zhao, J. Qin, K. Bai, J. Yu, X. Zhang, *FlexMat* **2024**, *1*, 150. <https://doi.org/10.1002/flm2.27>